

Automatically Predict Material Properties with Microscopic Image: Example Polymer Compatibility

Zhilong Liang, Zhenzhi Tan, Ruixin Hong, Wanli Ouyang, Jinying Yuan* and Changshui Zhang*

Abstract: Many material properties are manifested in the morphological appearance and characterized with microscopic image, such as scanning electron microscopy (SEM). Polymer compatibility is a key physical quantity of polymer material and commonly and intuitively judged by SEM images. However, human observation and judgement for the images is time-consuming, labor-intensive and hard to be quantified. Computer image recognition with machine learning method can make up the defects of artificial judging, giving accurate and quantitative judgement. We achieve automatic compatibility recognition utilizing convolution neural network and transfer learning method, and the model obtains up to 94% accuracy. We also put forward a quantitative criterion for polymer compatibility with this model. The proposed method can be widely applied to the quantitative characterization of the microstructure and properties of various materials.

Key words: Machine Learning, Transfer Learning, Polymer Compatibility, SEM, Computer Image Recognition

1. Introduction

The methods to computing and characterizing material properties have developed rapidly in recent years. In terms of material property calculations, methods such as molecular dynamics (MD) simulations achieved good results in free energy calculation^{1, 2} and drug discovery^{3, 4}. In addition to material property calculation, material property characterization is also a crucial part of material researches. Among kinds of characterization methods, scanning electron microscopy (SEM) is one of the most important means from observe microscopic image to determine macroscopic and intrinsic properties of the materials. At the present stage, this relies heavily on human observation and judgement, which is time-consuming, labor-intensive and hard to be quantified. The development of artificial intelligence and machine learning makes automatic image recognition applicable⁵. With the help of computer image recognition technology, we could build an effective bridge from the microgram to the macroscopic properties. Allen et al.⁶ used convolution neural network (CNNs) to identify the common functional groups in gas-phase FTIR (Fourier transform infrared spectroscopy), simplified the recognition process of infrared spectrum. Lee et al.⁷ developed a GA-based image analysis method to accurately analyze the morphological properties of nanoparticles and achieved 99.75% accuracy. Gao et al.⁸ obtained the function model of material T_g and image characteristics through machine learning by extracting microscopic image features of materials.

However, directly bridging microscopic images and material macroscopic properties remains a challenge and worth exploring. Considering that polymer composite materials are important engineering materials and that their compatibility is a key index to determine their performance, we chose quantitative judgment of polymer compatibility with SEM images as an example. Polymer blend materials involve blending two or more polymers to produce a new material. These blends have been extensively researched due to their capacity to combine the advantageous properties of different polymers and their ease of synthesis and processing. Researchers have utilized machine

learning methods to investigate their properties, including the mechanical properties⁹, liquid crystal behavior¹⁰, thermal conductivity¹¹, dielectric constant¹², optical properties¹³ and molecular design¹⁴. Among all kinds of properties, polymer compatibility is the primary basis for determining the form, structure and properties of blends¹⁵, and it is difficult for incompatible polymers to form materials with good properties. Therefore, determining whether and how different polymers are compatible is a crucial question and attracts researchers' focus¹⁶. While the compatibility of some blends could be judged by their properties in physical chemistry, microscopic observation is the most efficient approach since this property is manifested in the homogeneity of morphological appearance. In general, compatible polymers have relatively smooth boundaries and a homogeneous phase, while incompatible polymers present clear phase separation and form a spherical dispersion phase or sea-island structure. Typical SEM images of polymer blends are shown in Fig.1. Figure A¹⁷ is the SEM image of a compatible polymer blend, in which two polymers form a homogeneous phase. Figure B¹⁸ is the SEM image of an incompatible polymer blend and presents clear phase separation. As previously mentioned, image judgment of polymer compatibility remains dependent on researcher completion and lacks a set of accurate and quantitative technical means to describe polymer compatibility. In this work, we presented an automated judging approach to improve efficiency and accuracy.

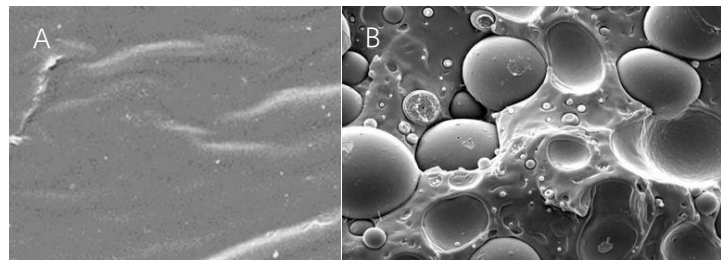


Figure 1. Typical SEM images of polymer blends. A¹⁷: compatible polymer blend. B¹⁸: incompatible polymer blend

We designed a deep neural network model to realize compatibility recognition with microscopic images of polymer blends. Also, we used transfer learning, a branch of machine learning to improve the prediction accuracy of the model. We collected 517 SEM images of polymers in total from the literature, combined with the PoLyInfo database¹⁹ and compatibility descriptions in the literature. Our model is pretrained in ImageNet²⁰ and then finetuned with the SEM images of polymer blends, which is so-called transfer learning. The model can give the judgment of polymer compatibility with 94% accuracy, making it possible to obtain the quantitative compatibility judgment index and establish a quantitative criterion of polymer compatibility. Our main contributions are:

(1) A machine learning framework (shown as Figure 2) is proposed to bridge material macroscopic properties and microscopic images. In the compatibility recognition task, we achieved 94% accuracy, which is comparable to the determination of researchers. It automates the morphology analysis of polymer blending materials and facilitates the development of high-throughput polymer experiments.

(2) A specific polymer compatibility image database is built, including SEM images, original descriptions in literature, and the microscopic scale. It will help researchers study polymer blend morphology and conduct downstream tasks.

(3) A quantitative criterion for polymer compatibility is established. This quantitative description will facilitate to study other properties of polymer blend related to compatibility.

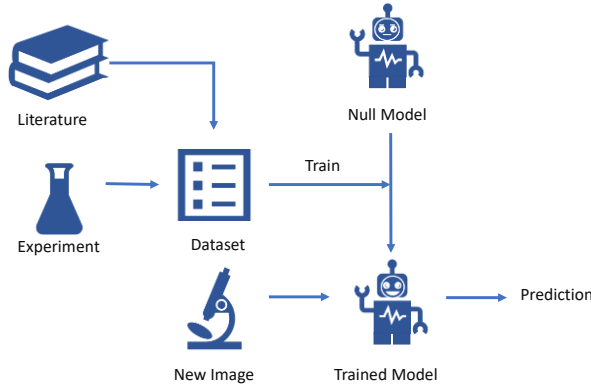


Figure 2. The machine learning framework to bridge material macroscopic properties and microscopic images

2. Methods

2.1. Dataset

Dataset plays a crucial important role in machine learning and needs to be accurate²¹. We extracted 517 original pictures from 687 pieces of literature about polymer compatibility and labeled their compatibility according to the PolyInfo¹⁹ database and literature descriptions. PolyInfo is a polymer database from NIMS that provides data for the design of various polymer materials. The morphology, characteristics of material, mixing or blending method, component ratio, and references of polymer blends were collected from the PolyInfo database. Through automatic screening, 8625 images were obtained from the literature, and 517 SEM images describing the compatibility of blends were manually screened. The compatibility was marked based on the PolyInfo and the descriptions in the literature. Since the descriptions of compatibility in literature and the PolyInfo database are mainly divided into compatibility and incompatibility, we treat compatibility prediction as a classification problem. The compatibility was labeled as compatible, incompatible, partially compatible. We also recorded the scale of SEM images of different polymers.

Table 1. Statistics of Dataset

Size	Split *	
	Training-set	Test-set
Raw Image	517	400 (78.8%)
Augmented	2,082	1,965 (51.9%)
		117 (86.3%)

* The figures in brackets mean the percentage of incompatible images.

In the data set, the ratio of compatible images to incompatible images is about 1:4. Statistics of dataset are shown in Table 1. In the training set, there are 85 compatible images and 315 incompatible images. To solve the problem of data imbalance and a small amount of data, we increased the amount of data in the training set through data augmentation to improve the generalization ability of the model. We augmented the compatible image by a factor of 12 and the incompatible image by a factor of 3 to try to balance both sides of the data as much as possible.

Augmentation operations included rotation, translation, flipping, and finally cropping to a size of 256 * 256, resulting in 1965 pieces of training data and 117 pieces of test data.

2.2. Model

Although many methods such as molecular dynamics, have been evaluated²² and used in micro-structure analysis convolution neutral network²³ (CNN) is a better choice in automatic image recognition since the development of image datasets (such as ImageNet²⁰) and computational power. Some kinds of model architectures with CNN module have been proposed. We designed a deep learning model based on VGG-Net²⁴ to meet our goals. At the same time, we applied some competing models to our dataset, including other deep learning algorithms such as Dense-Net²⁵ and Res-Net²⁶ and a traditional edge detection algorithm like Sobel. Details of these models are introduced as follows.

2.2.1. VGG-Net

CNN extracts different morphological features of the image through the convolution, and then pools the image, and finally gets the predicted result. VGG-Net was proposed by Oxford's Visual Geometry Group. VGG-Net uses two or three 2×2 or 3×3 convolution kernels to replace the larger convolution nuclei in the previous convolutional neural network. The stacked small convolution kernel can improve the depth of the network while maintaining the same receptive field, and more complex models can be learned through multi-layer nonlinear layers. Stacking small convolution kernels also reduces the number of model parameters and training costs. The VGG16 model (Figure 3A) used in this experiment contains 16 hidden layers (including 13 convolution layers and 3 fully connected layers), and the original 1000-dimensional soft-max is modified to 2-dimensional to describe the classification problem of compatibility.

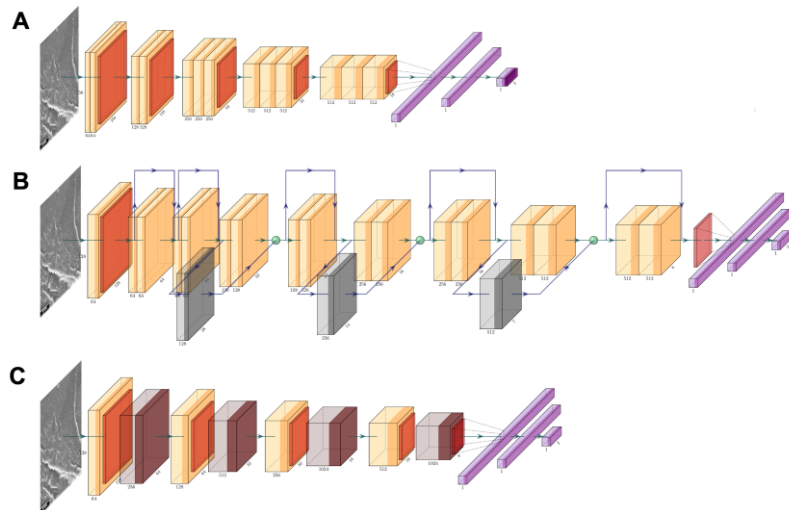


Figure 3. Diagram of CNN model used to predict polymer blends compatibility, in which yellow blocks represent the convolution layers, red blocks represent the pooling layers, and purple blocks represent the linear classification layer. In this experiment, the final classification layer was modified into 2-dimension to predicting the compatibility. A) VGG16; B) ResNet18, in which grey blocks represent shortcut connection block; C) DenseNet121, in which brown blocks represent Dense block.

2.2.2. Res-Net

It is widely believed that with the increase of the depth of the network, the fitting effect of the network on the function becomes better. However, Kaiming He et al. found that the accuracy of the model degrades with the deepening of the number of layers of the network, which they attribute to the fact that the depth of the network leads to the data being mapped to more discrete spaces, decreasing the fitting ability of simple mappings. So, they designed a ResNet model with "shortcut connection". Based on VGG model, ResNet added ResNet block, which changed the mapping from $F(x)$ to $F(x) + x$, improved the ability of the model to retain the identity transformation, so that the training of the deep model can be easier. The feature part of ResNet18(Figure 3B) is used to predict the polymer compatibility image, and the linear layer is modified.

2.2.3. Dense-Net

Based on ResNet, Gao Huang et al. proposed a densely connected mechanism and got the DenseNet model. Each layer in DenseNet connect with all previous layers in the channel dimension, so for a network of layer L , DenseNet contains $\frac{L(L+1)}{2}$ connections in total. Since dense connections require consistent feature map sizes, DenseNet uses the structure of DenseBlock + Transition. DenseBlock adopts a dense connection mode within layers and reduces the image size through the Transition layer. DenseNet can achieve better results than ResNet in some cases while the parameters are greatly reduced. The feature part of Dense-Net121(Figure 3C) is used to predict the polymer compatibility image, and the linear layer is modified.

2.2.4. Sobel

The Sobel edge detection algorithm is a method to detect image edges. The edge is the abrupt change in grayscale gradient, which usually corresponds to the phase interface between different polymers in SEM images. The Sobel operator is the core of Sobel edge detection, which includes two sets of 3×3 matrices, which monitor the horizontal edge and the longitudinal edge, respectively. The greatest difference between Sobel and machine learning methods above is that the Sobel operator is fixed while convolution cores in machine learning are learnable. By convolving the Sobel operator with the plane graph, the approximate values of the lateral and longitudinal brightness difference can be obtained, which shows the edges in the pictures²⁷ shows the raw image and the image processed by the Sobel algorithm.

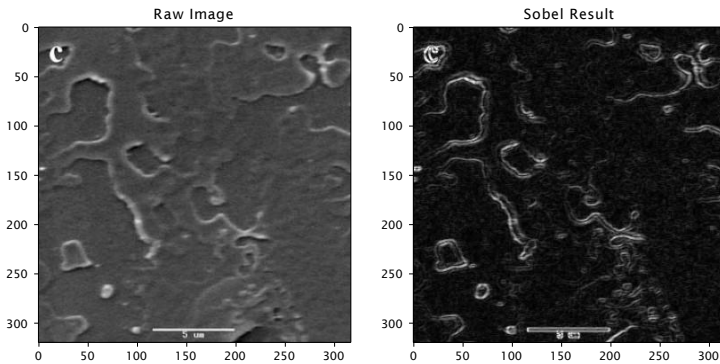


Figure 4. Comparison of Raw Image²⁷ and Sobel Image.

2.3. Transfer Learning

Transfer learning, as a widely used machine learning method, can significantly improve the performance of the model, especially in the fields of natural language processing and image recognition. Transfer learning aims to extract knowledge from source tasks and data (which is called ‘pretrain’), and then apply that knowledge to target tasks (which is called ‘finetune’).²⁸ Instead of learning the task from zero, transfer learning techniques try to transfer knowledge from the pretraining process when there is less high-quality training data for the target task. We applied transfer learning methods by utilizing the models pretrained with ImageNet images in advance and finetuning the classification parameters with the SEM images. It’s assumed that the model can learn the patterns from millions of images in the pretraining process and converge faster on our data.

2.4. Experiment Setting

We conducted all experiments in Python using Pytorch toolbox, and the computing was accelerated on a NVIDIA GeForce RTX 2080 Ti GPU. We set the maximal training epoch number to 100 and the mini-batch to 128. The initial learning rate was set to 10^{-4} . The total time spent was about 10 min for a complete training of 100 iterations. The Adam optimizer²⁹ was used to optimize the loss function. As for criterion, we chose cross-entropy as the loss function since it’s a binary classification problem:

$$Loss = CrossEntropy(y, p) = \frac{1}{N} \sum_i -[y_i \log(p_i) + (1 - y_i) \log(1 - p_i)], \quad (1)$$

where p_i represents the probability of the sample i being compatibility-related.

Since we are accomplishing a classification prediction task, we also care about the accuracy of the model. In addition, we test some other indices:

$$Accuracy = (TP + TN) / (P + N), \quad (2)$$

$$Precision = TP / (TP + FP), \quad (3)$$

$$Recall = TP / (TP + FN), \quad (4)$$

$$Specificity = TN / (TN + FN), \quad (5)$$

$$F1\ score = 2 \times \frac{Precision \times Recall}{Precision + Recall}, \quad (6)$$

where P means compatible, N means incompatible, T means true, and F means false. Precision refers to the proportion of the “compatible” predictions that are truly compatible. Recall refers to the proportion of compatible samples with the correct prediction among all compatible samples. Specificity means the ability to predict incompatible cases. The $F1$ score comprehensively considers the effects of precision and recall. If one of them is too small, the value of $F1$ will become smaller.

3. Results

3.1. Competing Model

For each model, we conducted 20 experiments with different random seed. Besides, we invited 21 researchers to participate in our SEM images recognition. The researchers have adequate chemical knowledge and learned more details about polymer compatibility from literature and our dataset. The best results of the competing models and the average result of top-10 researchers are presented in Table 2. The accuracy of pretrained Dense-Net (91.45%) and pretrained Res-Net (90.60%) is

close to that of VGG-Net (94.02%), which shows the effectiveness of the deep learning models and convolution networks. We find that, except for the Sobel method, all pretrained models performed well on the test set, which got even higher scores than the researchers' results. The reason may be that the details in SEM images are difficult for researchers to distinguish in some cases, so researchers have to make subject decisions. In addition, labels in our dataset are determined with SEM and other examinations (such as DSC) to guarantee the correctness while researchers can only utilize the microscopic information. Image recognition model can recognize all details in SEM images and learn the complex relation between SEM images and compatibility, so perform better than our researchers.

Moreover, the specificity of all models is much higher than their precision. As explained in experiment setting, precision means the ability to predict compatible cases while specificity means the ability to predict incompatible cases. Hence, for different categories, all models pay more attention to incompatible images. The reason may be the unbalanced proportion of training data. Although we augmented the training data, the raw images still influence the effect of training process. The number of incompatible images is nearly four times as large as the number of compatible images.

Table 2. Results of Competing Models

Model	Test_Accu (%)	Train_Accu(%)	Precision (%)	Recall (%)	Specificity (%)	F_1 score (%)
Pre-VGG	94.02	99.44	81.25	76.47	97.00	78.78
Pre-Dense	91.45	99.85	71.43	62.50	96.04	66.67
Pre-Res	90.60	99.19	69.23	56.25	96.04	62.07
Sobel ¹	80.20	—	47.06	8.00	97.80	13.68
Researcher	83.88	—	47.17	76.25	85.10	57.23

1.Boundary of classifier in Sobel method is set to 18 to achieve the highest accuracy.

3.2. Ablation Results

We have shown the effectiveness of several deep learning models with the pretrained method. To verify the importance of pretrain process, we conducted ablation experiments where pretrained parameters of models were not used. All models were trained on our SEM images dataset ab initio. The results are listed in Table 3. Besides, we showed the statistical data of all 20 experiments in Figure 5.

Table 3. Comparison Results of Pretrained (Pre) and No-Pretrained (Nopre) Models

Model	Test_Accu (%)	Train_Accu (%)	Precision (%)	Recall (%)	Specificity (%)	F_1 score (%)
Nopre-VGG	87.18	55.47	100.00	6.25	100.00	11.76
Pre-VGG	94.02	99.44	81.25	76.47	97.00	78.78
Nopre-Dense	88.89	68.04	63.63	43.75	96.04	51.85
Pre-Dense	91.45	99.85	71.43	62.50	96.04	66.67
Nopre-Res	91.45	97.30	71.43	62.50	96.04	66.67
Pre-Res	90.60	99.19	69.23	56.25	96.04	62.07

It is clear that VGG-Net and Dense-Net both performed better when pretraining was conducted; they improved by 7% and 3%, respectively. It is also indicated in Figure 5. When models were no-pretrained, it's difficult to train them with only our dataset, and their accuracy is not higher than ratio of incompatible images in both training set and test set. It means they did not learn the correct rule and just assumed all images incompatible. We took the whole results in the training process and compare the models with and without pretrained method, and presented them in Figure 6.

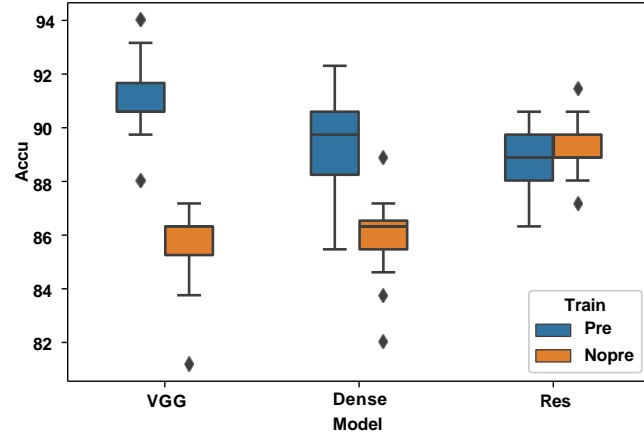


Figure 5. Box plot of the best accuracy in 20 experiments.

Average accuracy of pretrained method is higher than no-pretrained method for each model, which indicates the effectiveness of transfer learning.

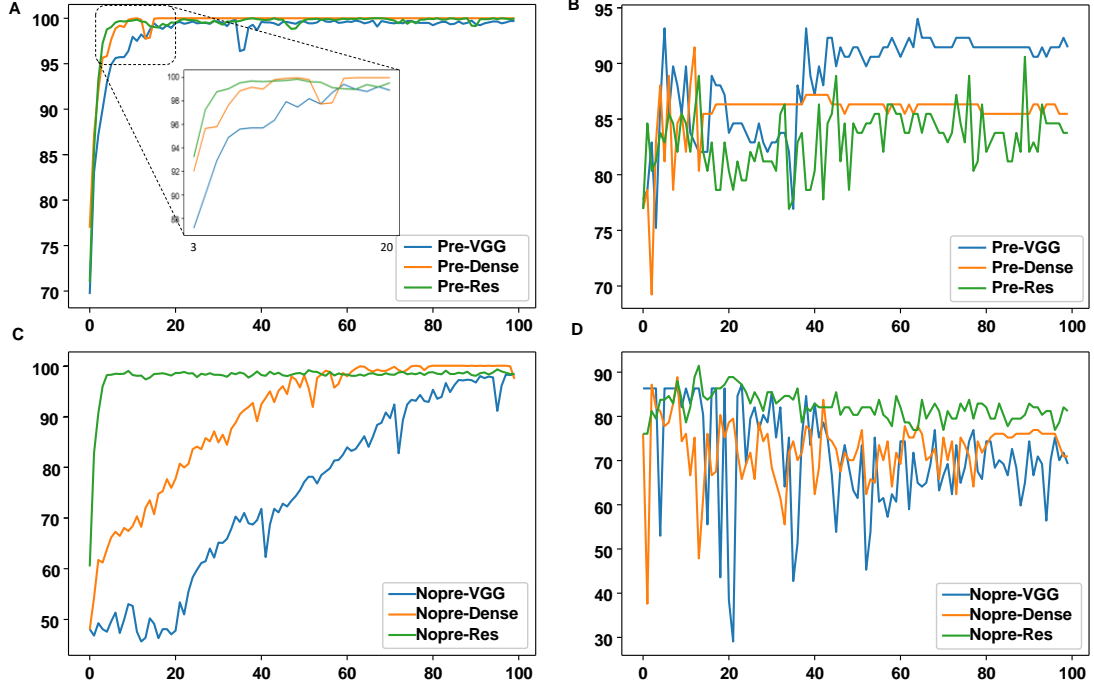


Figure 6. Accuracy of models on training set and test set in the training process. Abscissa means epochs.

- (A) Accuracy of pretrained models on training set.
- (B) Accuracy of pretrained models on test set.
- (C) Accuracy of no-pretrained models on training set.
- (D) Accuracy of no-pretrained models on test set.

As presented in Figure 5, we can find several interesting results. As to the training set, a pretrained model can rapidly converge and reach nearly 100% accuracy, while a no-pretrained model has to experience a relatively long process. This indicates that through pretraining, models reserved some basic knowledge so that when they were transferred to a new dataset, they could rapidly adjust parameters to solve the problem. As to the test set, we can also find that the pretrained models have a clearer and steadier optimizer process, while no-pretrained models fluctuate wildly. These results prove the effectiveness of the transfer learning method.

Furthermore, we can see that the rates of convergence on the training set differ during these untrained models. Res-Net without pretraining can converge rapidly on the training set, which is close to pretrained Res-Net, while no-pretrained Dense-Net and VGG-Net converge much more slowly than pretrained models. The difference may come from the model architecture and the connections between different layers in Res-Net and Dense-Net. The difference is connected with the result on the test set. We can find that no-pretrained Res-Net performs better than pretrained Res-Net. Meanwhile, the convergence rate gap between the no-pretrained and pretrained methods of Dense-Net and Res-Net is consistent with prediction accuracy on the test set. (2% for Dense-Net and 7% for VGG-Net)

3.3. Case Study and Quantitative Criterion

In order to investigate the methodology of our prediction model, we conducted a case study. We randomly chose 8 SEM images^{30, 31} (Figure 7) in our dataset and the best prediction model, the pretrained VGG-Net, with 94% accuracy on the test set. We processed these images using the best model and obtained the prediction results. Labels and predictions for these images are listed in Table 4.

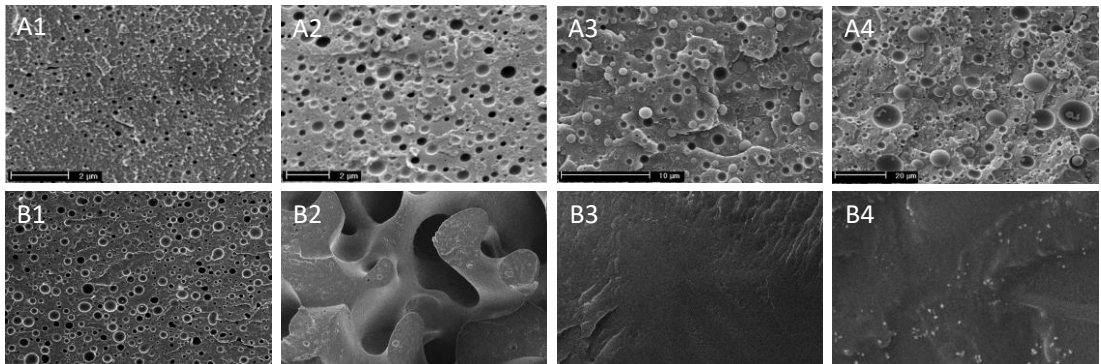


Figure 7. SEM images for case study. A1-A4 show micrographs of the PMMA/PS1 and PMMA/PP blends³⁰. B1-B4 show SEM pictures of annealed and unannealed blends of PTT/PC³¹.

From Table 4, we can find that the prediction result is consistent with the compatibility information. For SEM images A1-A4, the samples are all incompatible, although the degree of incompatibility is different. From these images, the particle diameter is listed in Table 4. From A1 to A4, the diameter increases, which indicates that the incompatibility increases. Through our model, we obtained the output for each image, including two categories. The final prediction is the SoftMax result of the two outputs, which means the probability of incompatibility. We can find that the prediction value also increases from A1 to A4. This result is consistent with the degree of

incompatibility.

Table 4. Results of Case Study

Image	Label	Particle Diameter	Output for Incompatible	Output for Compatible	Prediction for Incompatibility ¹
A1	Incompatible	0.24 μm	0.08	-30	$e^{0.08}/(e^{0.08} + e^{-30})$
A2	Incompatible	0.50 μm	0.22	-47	$e^{0.22}/(e^{0.22} + e^{-47})$
A3	Incompatible	1.49 μm	0.48	-47	$e^{0.48}/(e^{0.48} + e^{-47})$
A4	Incompatible	2.28 μm	-0.29	-124	$e^{-0.29}/(e^{-0.29} + e^{-124})$
B1	Incompatible	—	0.23	-67	$e^{0.23}/(e^{0.23} + e^{-67})$
B2	Incompatible	—	0.16	-89	$e^{0.16}/(e^{0.16} + e^{-89})$
B3	Compatible	—	-41	10	$e^{-41}/(e^{-41} + e^{-10})$
B4	Compatible	—	-32	8	$e^{-32}/(e^{-32} + e^8)$

1. Prediction for Incompatibility is SoftMax result of Output for Incompatible and Compatible

As for B1-B4, these images include both compatible and incompatible samples. The particle information is not clear, but we can compare the outputs and predictions for different categories. The outputs for incompatible are both negative for B1 and B2, while positive for B3 and B4. It is obvious the predictions for incompatibility are all consistent with the labels. Through the case study above, the effectiveness of our model is shown, the quantitative criterion for polymer compatibility is presented.

4. Conclusion

In this work, we presented a machine learning framework to bridge material microscopic images and macroscopic properties. Start with polymer compatibility recognition, machine learning method was introduced into the materials field. We achieved 94% accuracy and presented a quantitative criterion for compatibility and conduct a case study to show its effectiveness.

Our research also yielded some intriguing results. Different deep learning models perform differently in the pretraining process, and it shows consistency with the final accuracy on the test set. As to the quantitative criterion, the result now shows polarization. Quantitative result of compatible sample is very close to '1' while it is close to '0' for incompatible samples.

Our method may still have some limitations, which can be improved in the future work. The performance of this method is constrained by the quality and clarity of SEM images. In SEM images, the convex of fracture surface is similar to the phase separation, which makes it different to distinguish its compatibility.

This work is an attempt to make the characterization of chemical experiments more automatic and intelligent. For example, researchers can continue to explore predict material yield stress, Young modulus, and other mechanical properties through SEM images. In addition, other chemical examination results can be analyzed through machine learning method, such as infrared spectroscopy etc. We believe that it will inspire more creative methods and promote the development of the interdisciplinary.

Data and Software Availability

The data and main code to reproduce the results of this study are available at following GitHub page: <https://github.com/Zhilong-Liang/Polymer-Compatibility-Image-Recognition>.

Supporting Information

Supplemental figure describing the confusion matrix of several models on the test set and figure of violin plot of result of Sobel method.

Author Information

Corresponding Authors

Jinying Yuan - Key Lab of Organic Optoelectronics and Molecular Engineering of Ministry of Education; Department of Chemistry, Tsinghua University, Beijing, P. R. China. Email: yuanjy@tsinghua.edu.cn

Changshui Zhang - Institute for Artificial Intelligence, Tsinghua University (THUAI); Beijing National Research Center for Information Science and Technology (BNRist); Department of Automation, Tsinghua University, Beijing, P. R. China. Email: zcs@mail.tsinghua.edu.cn

Authors

Zhilong Liang - Institute for Artificial Intelligence, Tsinghua University (THUAI); Beijing National Research Center for Information Science and Technology (BNRist); Department of Automation, Tsinghua University, Beijing, P. R. China.

Zhenzhi Tan - Department of Chemistry, Tsinghua University, Beijing, P. R. China.

Ruixin Hong - Institute for Artificial Intelligence, Tsinghua University (THUAI); Beijing National Research Center for Information Science and Technology (BNRist); Department of Automation, Tsinghua University, Beijing, P. R. China.

Wanli Ouyang - Shanghai AI Lab, Shanghai, P. R. China. Email: ouyangwanli@pjlab.org.cn

Author Contributions

Z.L., C.Z. and J.Y. conceived of the main research idea and carried out the method design and ML modeling. Z.T. took part in the literature summary and database building. R.H. and W.O. took part in the database building and revised the manuscript. C.Z. and J.Y. supervised the project and revised the manuscript. All authors discussed the results and commented on the manuscript.

Notes

The authors declare no competing financial interest.

Acknowledgement

This work is supported by a grant (no. 2021GQG1025) from the Guoqiang Institute, Tsinghua University, Beijing, China.

Reference

(1) Suruzhon, M.; Senapathi, T.; Bodnarchuk, M. S.; Viner, R.; Wall, I. D.; Barnett, C. B.; Naidoo, K. J.; Essex, J. W. ProtoCaller: Robust Automation of Binding Free Energy Calculations. *J. Chem. Inf. Model.*

2020, *60* (4), 1917-1921.

(2) Bonomi, M.; Branduardi, D.; Bussi, G.; Camilloni, C.; Provati, D.; Raiteri, P.; Donadio, D.; Marinelli, F.; Pietrucci, F.; Broglia, R. A.; et al. PLUMED: A portable plugin for free-energy calculations with molecular dynamics. *Comput. Phys. Commun.* **2009**, *180* (10), 1961-1972.

(3) Durrant, J. D.; McCammon, J. A. Molecular dynamics simulations and drug discovery. *BMC Biology* **2011**, *9* (1), 71.

(4) Salo-Ahen, O. M. H.; Alanko, I.; Bhadane, R.; Bonvin, A. M. J. J.; Honorato, R. V.; Hossain, S.; Juffer, A. H.; Kabedev, A.; Lahtela-Kakkonen, M.; Larsen, A. S.; et al. Molecular Dynamics Simulations in Drug Discovery and Pharmaceutical Development. *Processes* **2021**, *9* (1), 71.

(5) Pak, M.; Kim, S. A review of deep learning in image recognition. In *2017 4th International Conference on Computer Applications and Information Processing Technology (CAIPT)*, 8-10 Aug. 2017, **2017**; pp 1-3.

(6) Enders, A. A.; North, N. M.; Fensore, C. M.; Velez-Alvarez, J.; Allen, H. C. Functional Group Identification for FTIR Spectra Using Image-Based Machine Learning Models. *Anal. Chem.* **2021**, *93* (28), 9711-9718.

(7) Lee, B.; Yoon, S.; Lee, J. W.; Kim, Y.; Chang, J.; Yun, J.; Ro, J. C.; Lee, J.-S.; Lee, J. H. Statistical Characterization of the Morphologies of Nanoparticles through Machine Learning Based Electron Microscopy Image Analysis. *ACS Nano* **2020**, *14* (12), 17125-17133.

(8) Xu, H.; Ma, S.; Hou, Y.; Zhang, Q.; Wang, R.; Luo, Y.; Gao, X. Machine Learning-Assisted Identification of Copolymer Microstructures Based on Microscopic Images. *ACS Appl. Mater. Interfaces* **2022**, *14* (41), 47157-47166.

(9) Gu, Y.; Lin, P. R.; Zhou, C. D.; Chen, M. Machine learning-assisted systematical polymerization planning: case studies on reversible-deactivation radical polymerization. *Sci China Chem* **2021**, *64* (6), 1039-1046.

(10) Leon, F.; Curteanu, S.; Lisa, C.; Hurd, N. Machine learning methods used to predict the liquid-crystalline behavior of some copolyethers. *Mol. Cryst. Liq. Cryst.* **2007**, *469*, 1-22.

(11) Wu, S.; Kondo, Y.; Kakimoto, M.-A.; Yang, B.; Yamada, H.; Kuwajima, I.; Lambard, G.; Hongo, K.; Xu, Y.; Shiomi, J.; et al. Machine-learning-assisted discovery of polymers with high thermal conductivity using a molecular design algorithm. *NPJ Comput. Mater.* **2019**, *5* (1).

(12) Liang, J. C.; Xu, S. Q.; Hu, L. F.; Zhao, Y.; Zhu, X. Machine-learning-assisted low dielectric constant polymer discovery. *Mater. Chem. Front.* **2021**, *5* (10), 3823-3829.

(13) Ye, S.; Meftahi, N.; Lyskov, I.; Tian, T.; Whitfield, R.; Kumar, S.; Christofferson, A. J.; Winkler, D. A.; Shih, C.-J.; Russo, S.; et al. Machine learning-assisted exploration of a versatile polymer platform with charge transfer-dependent full-color emission. *Chem* **2023**.

(14) Du, S.; Wang, X.; Wang, R.; Lu, L.; Luo, Y.; You, G.; Wu, S. Machine-learning-assisted molecular design of phenylnaphthylamine-type antioxidants. *Physical Chemistry Chemical Physics* **2022**, *24* (21), 13399-13410.

(15) Krause, S. Polymer Compatibility. *Journal of Macromolecular Science, Part C: Polymer Reviews* **1972**, *7* (2), 251-314.

(16) Liang, Z. L.; Li, Z. W.; Zhou, S.; Sun, Y. W.; Yuan, J. Y.; Zhang, C. S. Machine-learning exploration of polymer compatibility. *Cell Rep. Phys. Sci.* **2022**, *3* (6).

(17) Wang, L. S.; Zhang, Z. P.; Chen, H. C.; Zhang, S. L.; Xiong, C. D. Preparation and characterization of biodegradable thermoplastic Elastomers (PLCA/PLGA blends). *J. Polym. Res.* **2010**, *17* (1), 77-82.

(18) Li, Y. J.; Shimizu, H. Improvement in toughness of poly(L-lactide) (PLLA) through reactive

blending with acrylonitrile-butadiene-styrene copolymer (ABS): Morphology and properties. *Eur. Polym. J.* **2009**, *45* (3), 738-746.

(19) Otsuka, S.; Kuwajima, I.; Hosoya, J.; Xu, Y.; Yamazaki, M. PoLyInfo: Polymer Database for Polymeric Materials Design. In *2011 International Conference on Emerging Intelligent Data and Web Technologies*, 7-9 Sept. 2011, **2011**; pp 22-29.

(20) Deng, J.; Dong, W.; Socher, R.; Li, L. J.; Kai, L.; Li, F.-F. ImageNet: A large-scale hierarchical image database. In *2009 IEEE Conference on Computer Vision and Pattern Recognition*, 20-25 June 2009, **2009**; pp 248-255.

(21) Sieg, J.; Flachsenberg, F.; Rarey, M. In Need of Bias Control: Evaluating Chemical Data for Machine Learning in Structure-Based Virtual Screening. *J. Chem. Inf. Model.* **2019**, *59* (3), 947-961.

(22) Zuo, X.; Cui, G.; Merz, K. M.; Zhang, L.; Lewis, F. D.; Tiede, D. M. X-ray diffraction “fingerprinting” of DNA structure in solution for quantitative evaluation of molecular dynamics simulation. *Proc. Natl. Acad. Sci.* **2006**, *103* (10), 3534-3539.

(23) Ciresan, D.; Meier, U.; Schmidhuber, J. Multi-column deep neural networks for image classification. In *IEEE Conference Computer Vision and Pattern Recognition*, **2012**; pp. 3642–3649.

(24) Simonyan, K.; Zisserman, A. Very Deep Convolutional Networks for Large-Scale Image Recognition. *CoRR* **2015**, *abs/1409.1556*.

(25) Huang, G.; Liu, Z.; Van Der Maaten, L.; Weinberger, K. Q. Densely connected convolutional networks. In *Proceedings of the IEEE conference on computer vision and pattern recognition*, **2017**; pp 4700-4708.

(26) He, K.; Zhang, X.; Ren, S.; Sun, J. Deep residual learning for image recognition. In *Proceedings of the IEEE conference on computer vision and pattern recognition*, **2016**; pp 770-778.

(27) Narkis, M.; Shach-Caplan, M.; Haba, Y.; Silverstein, M. S. PVC modification through polymerization of a monomer absorbed in porous suspension-type PVC particles. *J. Vinyl Addit. Technol.* **2004**, *10* (3), 109-120.

(28) Pan, S. J.; Yang, Q. A Survey on Transfer Learning. *IEEE Transactions on Knowledge and Data Engineering* **2010**, *22* (10), 1345-1359.

(29) Kingma, D. P.; Ba, J. Adam: A Method for Stochastic Optimization. *CoRR* **2014**, *abs/1412.6980*.

(30) Calvão, P. S.; Yee, M.; Demarquette, N. R. Effect of composition on the linear viscoelastic behavior and morphology of PMMA/PS and PMMA/PP blends. *Polymer* **2005**, *46* (8), 2610-2620.

(31) Aravind, I.; Eichhorn, K.-J.; Komber, H.; Jehnichen, D.; Zafeiropoulos, N. E.; Ahn, K. H.; Grohens, Y.; Stamm, M.; Thomas, S. A Study on Reaction-Induced Miscibility of Poly(trimethylene terephthalate)/Polycarbonate Blends. *J. Phys. Chem. B* **2009**, *113* (6), 1569-1578.